



PAPER • OPEN ACCESS

## Effect of Y/Zn ratio on microstructure and properties of as-extruded Mg-Y-Zn alloys

To cite this article: Baosheng Liu *et al* 2020 *Mater. Res. Express* **7** 036530

View the [article online](#) for updates and enhancements.

You may also like

- [The microstructure and mechanical properties of Mg-Gd-Y-Zn-Zr system and Mg-Gd-Y-Zr system alloys by RUE deformation](#)  
Leichen Jia, Jianmin Yu, Wenlong Xu et al.
- [The evolution of LPSO phase and its influence on grain size during cooling free forging](#)  
Guoqiang Wang, Zhongliang Xiao, Zhen Yang et al.
- [Thermal compression, processing maps and microstructural evolution of as-cast Mg-Gd-Y-Zn-Zr alloy with long period stacking ordered phase](#)  
Zhiyong Xue, Wenbo Luo, Zhi Zhao et al.

**ECS**  
The  
Electrochemical  
Society  
Advancing solid state &  
electrochemical science & technology

**DISCOVER**  
how sustainability  
intersects with  
electrochemistry & solid  
state science research

## Materials Research Express



## PAPER

## Effect of Y/Zn ratio on microstructure and properties of as-extruded Mg-Y-Zn alloys

## OPEN ACCESS

## RECEIVED

1 January 2020

## REVISED

6 March 2020

## ACCEPTED FOR PUBLICATION

17 March 2020

## PUBLISHED

30 March 2020

Original content from this work may be used under the terms of the [Creative Commons Attribution 4.0 licence](#).

Any further distribution of this work must maintain attribution to the author(s) and the title of the work, journal citation and DOI.

Baosheng Liu<sup>1,2</sup> , Jiaao Yang<sup>1,2</sup>, Zehui Wang<sup>1,2</sup> and Daqing Fang<sup>1,2,3</sup><sup>1</sup> College of Materials Science and Engineering, Taiyuan University of Science and Technology, Taiyuan, People's Republic of China<sup>2</sup> Engineering Research Center for Magnesium Alloys of Shanxi Province, Taiyuan University of Science and Technology, Taiyuan, People's Republic of China<sup>3</sup> State Key Laboratory for Mechanical Behavior of Materials, Xi'an Jiaotong University, Xi'an, People's Republic of ChinaE-mail: [fangdaqing@xjtu.edu.cn](mailto:fangdaqing@xjtu.edu.cn)**Keywords:** extruded Mg-Y-Zn, LPSO phase, microstructure, mechanical properties, corrosion behavior**Abstract**

In this work, four Mg-Y-Zn alloys with specific Y/Zn (wt%) ratio have been prepared. The effects of Y/Zn (wt%) on the microstructure of extruded Mg-Y-Zn alloy were investigated by SEM and TEM. The mechanical properties and corrosion behavior of extruded Mg-Y-Zn alloy were also studied by tensile test, electrochemical and immersion measurements. The corrosion mechanism was studied by SEM observation of the surface morphology of the samples after immersion corrosion. The result indicates that the as-extruded Mg-6Y-3Zn alloy consists of  $\alpha$ -Mg, W phase and long-period stacking ordered structure (LPSO) phases. Two types of LPSO structure (18 R and 14 H) appear in the as-extruded alloys. The volume fraction of LPSO increases with the increase of Y and Zn atoms with the same Y/Zn mass ratio. Mg-9Y-3Zn alloy has the best comprehensive mechanical properties. Its yield strength, ultimate tensile strength and elongation are 230 MPa, 327 MPa and 23% respectively, because the volume fraction of LPSO phase in the alloy is the highest. In addition, the higher volume fraction of LPSO is beneficial to enhance the corrosion resistance of Mg-9Y-3Zn alloy.

Magnesium alloys have a series of performance advantages, such as low density, good specific strength and stiffness, good casting performance and processing performance, and also has low elastic modulus, vibration and noise reduction, etc, which have been widely applied in 3 C, aerospace and automobile fields [1–3]. However, the unavoidable problem is the low strength and poor corrosion resistance of magnesium alloys [4–6]. Therefore, researchers have done a lot of research on the strengthening and corrosion behavior of magnesium alloys [7–10].

In improving the strength of magnesium alloys, magnesium rare earth alloys are the most successful systems. Recent studies have found that adding a small amount of Zn to certain Mg-RE alloys can generate a novel long-period stacking ordered structure (referred to as long-period structure, LPSO structure) under appropriate addition amounts and process conditions. In-depth research shows that there are three types of ternary equilibrium phases in Mg-Zn-Y alloys, which are  $Mg_3YZn_6$  (I-phase icosahedral quasi-crystal structure and quasi-periodic order),  $Mg_3Y_2Zn_3$  (W-phase face-centered cubic structure) and  $Mg_{12}ZnY$  (X-phase long period stacked ordered structure, including 6 H, 14 H and 18 R) [8]. At the same time, it is generally believed that the phase composition of the alloy depends on the Y/Zn molar ratio [9]. It is reported that LPSO is an important strengthening phase in Mg-Y-Zn alloy, and the common structures are 18 R and 14 H [10]. After heat treatment at 350 °C–500 °C, 18 R structure will be transformed into 14 H LPSO structure [11]. Wang J *et al* reported that the LPSO structural phase can improve the mechanical properties of magnesium alloys while maintaining the good damping capacity of the alloys, and the LPSO phase arranged along the extrusion direction can act as the hardening phase [12]. It is known that hot extrusion is an effective processing technique for improving the mechanical properties of magnesium alloys containing LPSO phase. During extrusion, recrystallized Mg grains improve the ductility and dispersion of the fibrous LPSO phase and contribute to the strengthening of the extruded Mg-Zn-Y alloy phase [13].

At the same time, the effect of LPSO on corrosion behavior in magnesium alloys has also been studied. For example, Zhang *et al* [14] found that the LPSO phase in extruded alloys can greatly improve the corrosion resistance of the alloys, and the corrosion resistance is enhanced as the volume fraction of the LPSO phase increases. However, it has also been reported [15] that LPSO in extruded alloys accelerated the corrosion of the alloy, and with the increase of LPSO phase volume fraction, the degradation rate of the alloy accelerated. In addition, Li *et al* [16] found that the corrosion resistance of magnesium alloys weakened first and then increased with the increase of LPSO phase volume fraction. It can be seen that the influence of corrosion behavior of LPSO on magnesium alloy has not been universally recognized.

In conclusion, Mg-Y-Zn alloys have attracted much attention due to their excellent performance and relatively low cost [6, 7]. However, most studies have focused on the microstructure and properties of a particular alloy. A series of Mg-Y-Zn alloys with different Y/Zn mass ratios were designed to study the effects of Y/Zn mass ratio on microstructure, mechanical properties and corrosion behavior of Mg-Y-Zn alloys.

## 1. Experiment

Mg-xY-yZn ( $x = 6,9$ ,  $Y = 1,3$ ) alloys were prepared by melting the raw materials pure Mg(99.9%), pure Zn(99.9%) and Mg-Y intermediate alloys in an electric furnace, using mixed gas ( $\text{CO}_2 + \text{SF}_6$ ) as protective gas at 750 °C and pouring them into a cylinder steel mold with diameter of 90 mm. The materials were recorded as WZ63, WZ93, WZ61 and WZ91. After the homogenization treatment at 400 °C for 10 h, the 650t oil press was used for extrusion. The extrusion temperature was 380 °C, and the test bar with a diameter of 20 mm was extruded. The extrusion ratio is 20:1 and the extrusion speed is  $1 \text{ m min}^{-1}$ .

The microstructure of the samples was observed by using FEI Quanta FEG 250 field emission scanning electron microscope (SEM), JEOL JEM 2100HT transmission electron microscope (TEM) and JEOL JEM-ARM 200 F condenser with spherical aberration correction. The samples were prepared by traditional polishing technique. The backscattering of the extruded alloy is obtained from the longitudinal section parallel to the extrusion direction. Image-Pro-Plus-6.0 software was used to calculate the volume fraction of LPSO phase in the alloy.

The WDW-E100D micro-controlled electronic universal material testing machine was used for the tensile test. Tensile specimens with a gauge size of  $2 \times 3.5 \times 15 \text{ mm}$  were cut from the middle part of the extruded bar of Mg-Y-Zn systemic alloys with their length parallel to the extrusion direction. The tensile rate is  $0.9 \text{ mm min}^{-1}$ , and each sample shall be subject to at least three times of tensile test.

The corrosion behavior of the alloy was studied by electrochemical method. The experiment was conducted at room temperature with 3.5% NaCl solution as the corrosive medium. The sample area was  $10 \text{ mm} \times 10 \text{ mm}$ , and the remaining area was covered with epoxy resin. The VersaSTAT 4 electrochemical workstation into action potential polarization curve method and electrochemical impedance spectroscopy test, using the standard three electrode method, including saturated calomel reference electrode was, platinum electrodes are auxiliary electrodes, work samples, was the initial sample in solution of time 3 min, after being open circuit potential stability measurement again, scan rate of  $1.0 \text{ mV s}^{-1}$ .

Finally, the EI Quanta FEG 250 field emission scanning electron microscope equipped with an energy spectrometer was used to observe the surface corrosion morphology of the alloy after immersion in 3.5% NaCl solution.

## 2. Results and discussions

### 2.1. Microstructure

As shown in figure 1, SEM morphology of four as-cast alloys. It can be seen that the tissues of the four as-cast alloys are all composed of a black -Mg matrix and a second phase of a bright white lamellar, and the bright white lamellar phase is LPSO [17]. The LPSO phase in the alloy is distributed in a network along the grain boundary. With the increase of Y/Zn mass ratio, the LPSO phase first changes from discontinuous network distribution to continuous network distribution and then to discontinuous network distribution. Moreover, the width of LPSO phase also increases first and then decreases with the increase of Y/Zn mass ratio. Obviously, the LPSO phase content in WZ93 alloy is the highest, and the lamellar LPSO is almost continuous.

As shown in figure 2, the SEM micrographs of the four extruded alloys. After extrusion, the WZ63 alloy structure is composed of a black matrix, a pale LPSO phase and a small amount of bright white granular W phase, which is distributed around the strip phase. With the increase of Y/Zn mass ratio, the bright white particle W phase disappeared in WZ93 alloy. The LPSO phase, which was originally reticulated, was elongated and distributed in long strips along the extrusion direction. After extrusion, the LPSO of WZ93 alloy with the highest content of the second phase was wider and the phase spacing was narrower. No cracks appeared in the

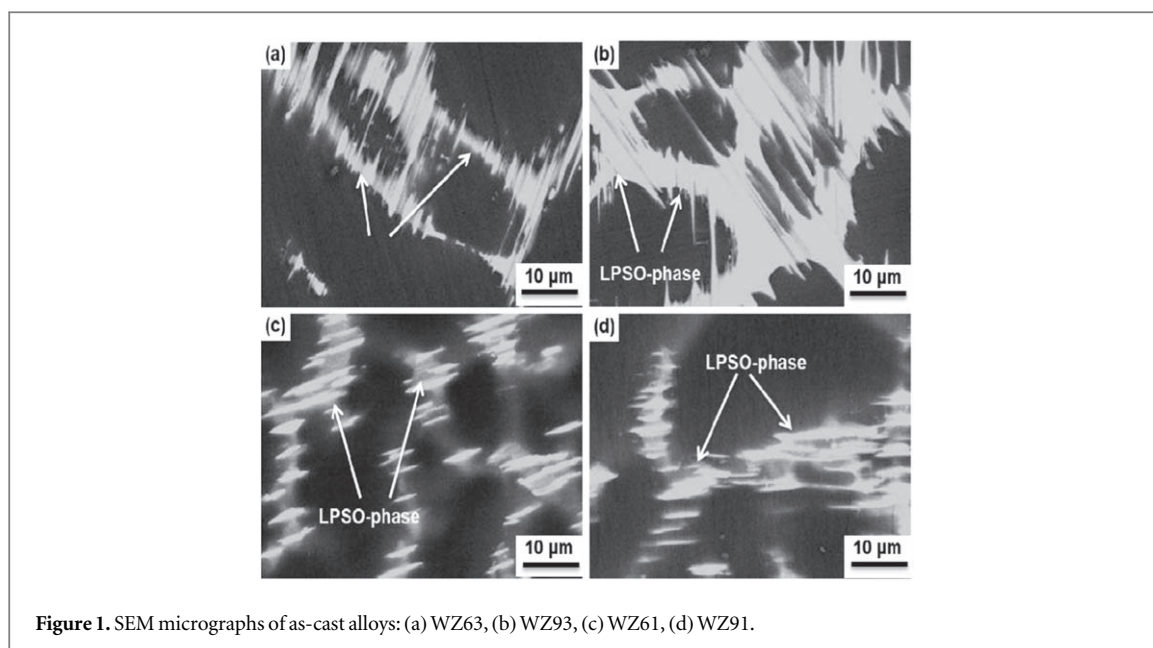


Figure 1. SEM micrographs of as-cast alloys: (a) WZ63, (b) WZ93, (c) WZ61, (d) WZ91.

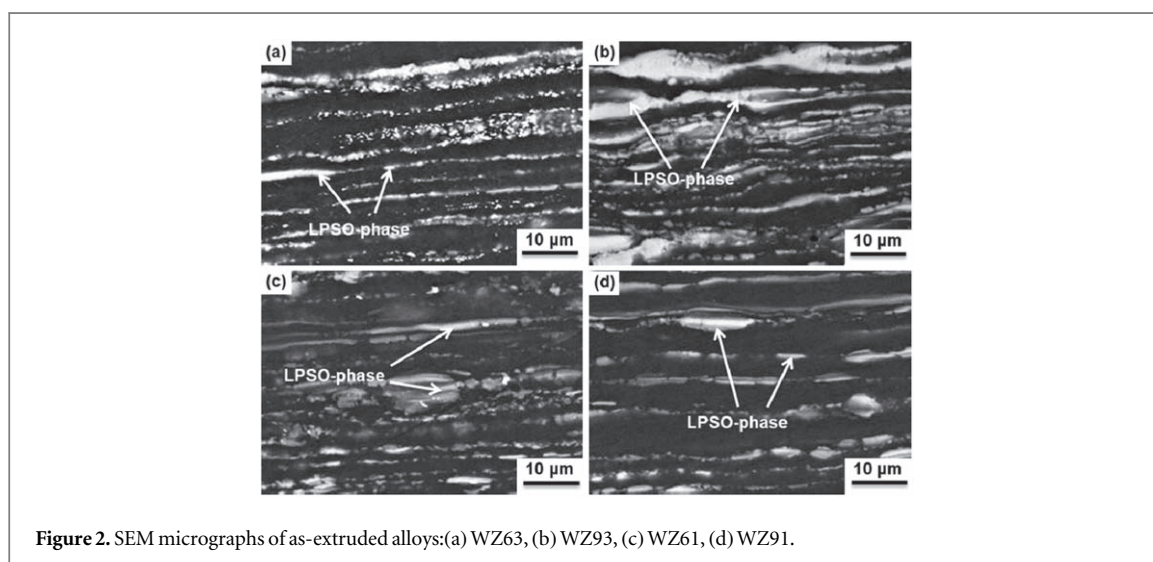


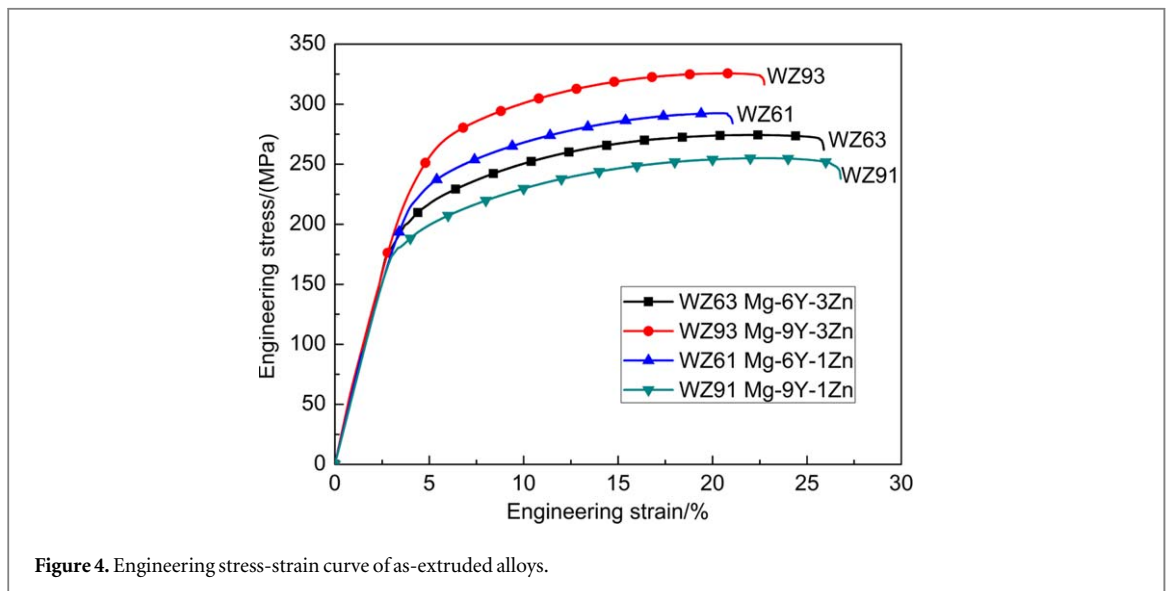
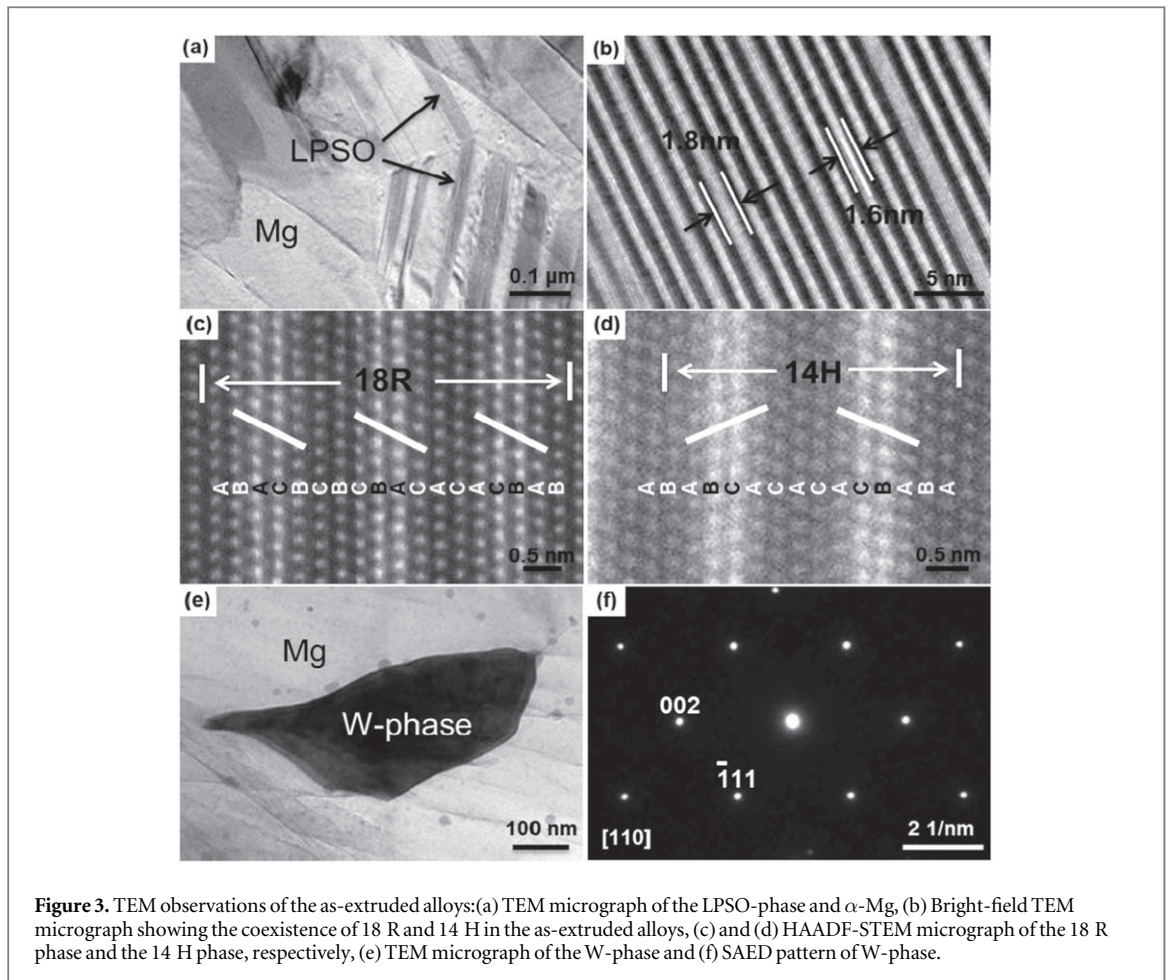
Figure 2. SEM micrographs of as-extruded alloys:(a) WZ63, (b) WZ93, (c) WZ61, (d) WZ91.

extruded LPSO phase, indicating that the LPSO phase in the alloy had good plasticity. According to the statistics, the volume fraction of LPSO in extruded WZ63, WZ93, WZ61 and WZ91 alloys is 28.12%, 43.02%, 35.26% and 22.15%, respectively. In general, the Y/Zn mass ratio determines the type of the second phase in the alloy. When the Y/Zn mass ratio is fixed, the total number of Y and Zn atoms determines the volume fraction of LPSO in the alloy.

As shown in figure 3, it is the TEM open field image of extruded WZ63 alloy. It can be seen that there are a large number of LPSO phases in  $\alpha$ -Mg matrix (in figure 3(a)), There are two different periods in the extruded samples. Their atomic stacking subcycles along the  $C$  axis were 1.6 nm and 1.8 nm, respectively (in figure 3(b)), which was consistent with the reported 18R-LPSO structure and 14H-LPSO structure [10]. The structure of the second phase was further characterized by high resolution spherical aberration electron microscopy, which proved to be typical of the LPSO phase, with a stacking order of 18 R times (figure 3(c)), consistent with previous reports [18]. In addition, as shown in figure 3(d), the 18 R structure is partially transformed into a 14H-LPSO structure during hot extrusion [19]. Figure 3(e) and f show the TEM image and SAED pattern along Mg matrix [110] in the extruded WZ63 alloy. It can be seen that the particle phase is W phase.

## 2.2. Mechanical properties

As shown in figure 4, it is the engineering stress-strain curve diagram of the four extruded samples. The ultimate tensile strength of extruded WZ63, WZ93, WZ61 and WZ91 alloys is 275 MPa, 327 MPa, 294 MPa and 255 MPa, respectively. Elongation was 26%, 23%, 21% and 27%, respectively. It can be seen in the figure 2 that with the



change of the total number of Y-Zn atoms, the content of LPSO phase in slender rod shape also changes accordingly. The tensile results show that the strength and plasticity of the alloy increase with the increase of LPSO phase.

WZ93 alloy with the largest volume fraction of LPSO phase has good comprehensive mechanical properties, mainly because the LPSO phase itself is the strengthening phase, and its strength, hardness and elastic modulus are significantly higher than the  $\alpha$ -mg matrix. After hot extrusion, the LPSO phase of the alloy showed a strip distribution along the extrusion direction, which can be regarded as the 'short fiber' reinforcing phase in the composite material, that is, the magnesium alloy was strengthened by 'short fiber strengthening mechanism'

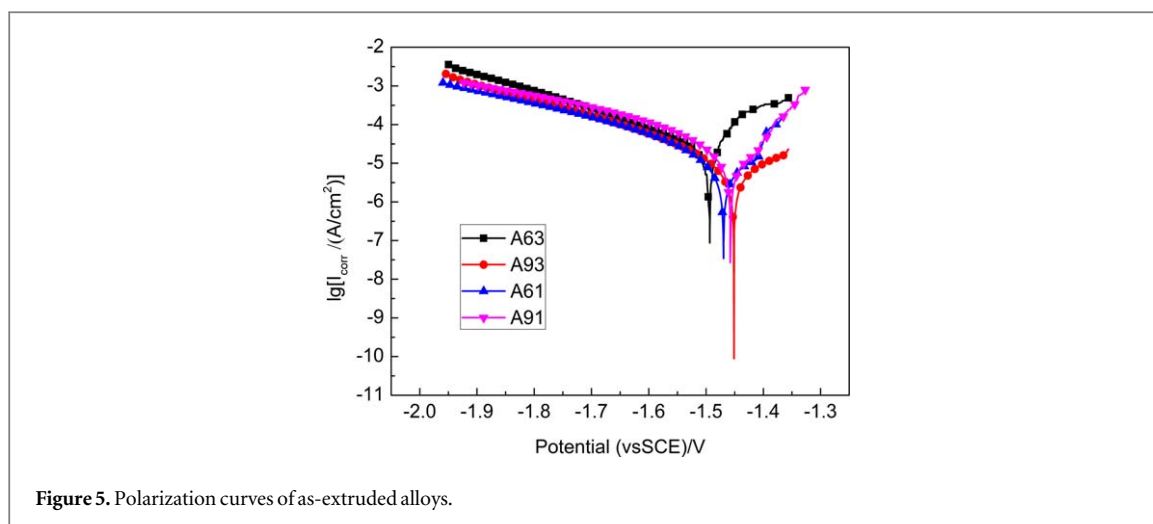


Figure 5. Polarization curves of as-extruded alloys.

Table 1. Fitting results of polarization curves.

No.	$E_{corr}/V$	$I_{corr}/(A \cdot cm^{-2})$
WZ63	-1.493	$3.110 \times 10^{-5}$
WZ93	-1.451	$1.575 \times 10^{-5}$
WZ61	-1.469	$2.489 \times 10^{-5}$
WZ91	-1.457	$6.041 \times 10^{-5}$

approximately. Also due to low slip system of LPSO phase, kinked LPSO phase is the main deformation mechanism, from the four kinds of alloy extrusion state of SEM image can be observed in torsion and bending LPSO phase (in figure 2), usually at the kink belt brought together a large number of dislocation, the dislocation with can further hinder dislocation motion, other more conducive to subsequent interaction of dislocation tangles, thus it can be reinforced magnesium alloys [20].

In the process of plastic deformation, microcracks are easy to grow at the interface of Mg/LSPO [21]. When the volume fraction of LSPO phase increases, more cracks are produced and the plasticity of the alloy decreases. Compared with WZ61 alloy, WZ93 alloy has the largest volume fraction of LPSO phase, but its elongation has increased. On the one hand, the bulk LPSO phase formed in WZ93 alloy reduces the interface between the two phases and reduces the probability of crack initiation. On the other hand, the kinking and bending of LSPO phase is more conducive to release the stress concentration and delay the crack growth.

### 2.3. Corrosion performance

As shown in figure 5, the Potentiodynamic polarization curves of the four extruded alloys are shown in table 1 which shows the fitting results of the polarization curves. It can be seen that WZ93 alloy has the maximum corrosion potential (-1.451 V) and the minimum corrosion current density ( $1.575 \times 10^{-5} A \cdot cm^{-2}$ ), indicating that WZ93 alloy has the best corrosion resistance [22, 23]. The comprehensive polarization curves and fitting results show that the corrosion resistance order of the four alloys is WZ93 > WZ61 > WZ63 > WZ91.

As shown in figure 6, it is the electrochemical impedance spectroscopy of the alloy. As can be seen from the figure, the Nyquist diagram is composed of a capacitive reactance arc located at a high frequency and an inductive reactance arc located at a low frequency. As the volume fraction of the LPSO phase increases, the capacitive reactance arc gradually increases, and the WZ93 alloy has the largest capacitive reactance radius. Capacitive arc is related to the charge transfer resistance and electric double layer capacitance during the corrosion process, that is, the larger the capacitive arc radius, the larger the charge transfer resistance, and the better the corrosion resistance. Therefore, it can be known from the electrochemical impedance spectroscopy that the corrosion resistance of the alloy is completely consistent with the result of the polarization curve.

As shown in figure 7, it is the equivalent circuit model of electrochemical impedance spectroscopy, and the fitting results are listed in table 2. In the equivalent circuit, R1 represents the solution resistance, R2 and CPE1 represent the charge transfer resistance and the double layer at the interface between Mg substrate and electrolyte solution, respectively, which is used to describe the capacitor ring at high frequencies. CPE1 is a constant phase Angle element and replaces the ideal capacitor to resolve the non-uniformity in the system, which is defined by the two values Y1 and n1. n1 is the dispersion index of CPE1, which reflects the roughness of

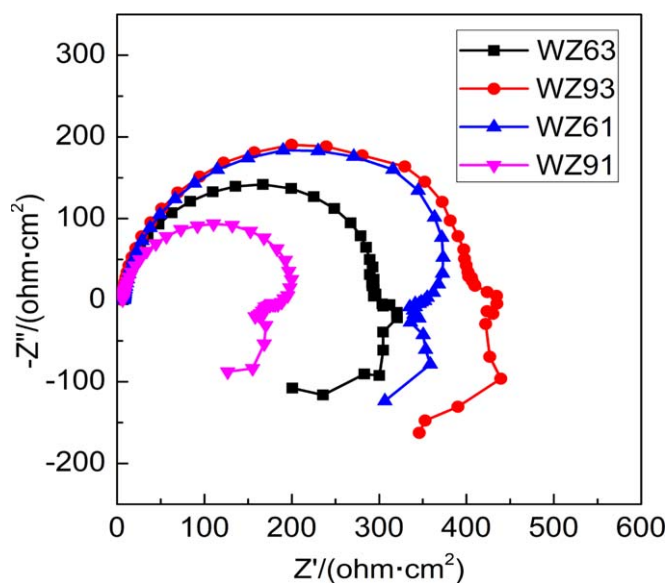


Figure 6. Electrochemical impedance spectroscopy of as-extruded alloys.



Figure 7. Equivalent circuit to fit electrochemical impedance spectroscopy of as-extruded alloys.

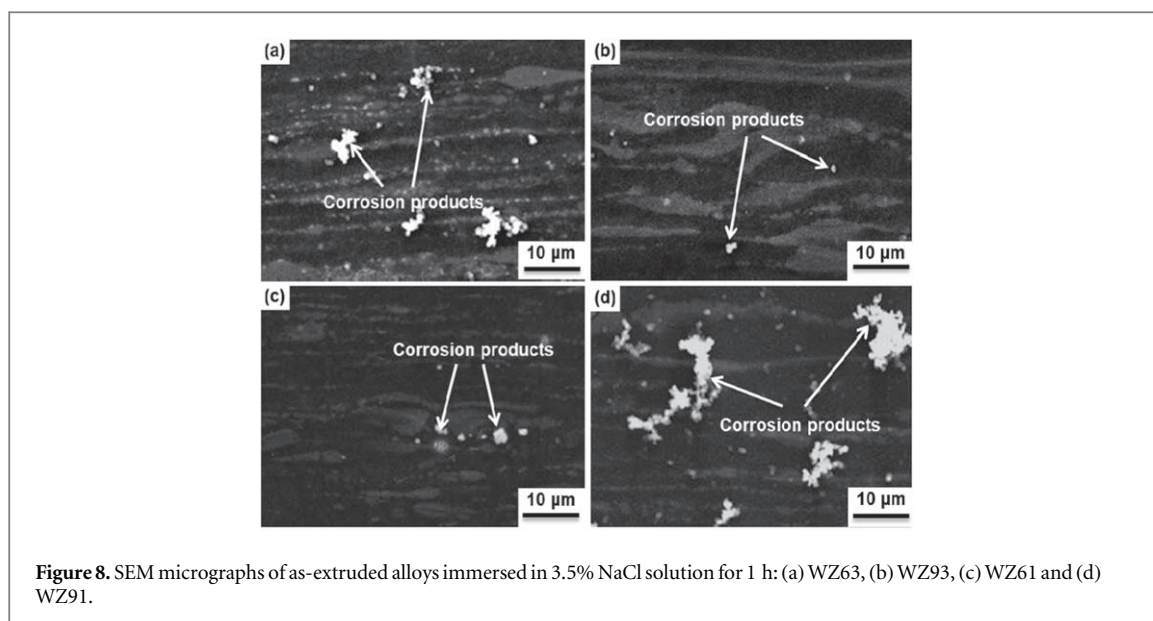
Table 2. Fitting results of electrochemical impedance spectroscopy.

No.	R1 ( $\Omega\text{cm}^2$ )	Y1 ( $\text{S}\cdot\text{secn}\text{cm}^{-2}$ )	n1	R2 ( $\Omega\text{cm}^2$ )	L1 ( $\text{Hcm}^{-2}$ )
WZ63	7.1	$1.307 \times 10^{-5}$	0.9488	298.9	832.3
WZ93	5.7	$1.419 \times 10^{-5}$	0.9428	416.8	1822.0
WZ61	7.6	$1.329 \times 10^{-5}$	0.9576	357.5	1964.0
WZ91	6.6	$1.615 \times 10^{-5}$	0.9420	181.7	589.0

the double layer. If  $n1 = 1$ , then CPE1 is the same as the capacitor; If  $n1 = 0$ , CPE1 represents the resistance. L1 represents the inductance and is used to describe the low frequency inductance loop, which indicates the beginning of local corrosion. Generally, a higher R2 value implies a lower dissolution rate of the Mg matrix. As can be seen from table 2, the R2 values of the four alloys are listed in the order from high to low: WZ93, WZ61, WZ63, and WZ91. Therefore, it indicates that the corrosion rate of the alloys increases in the order of WZ93, WZ61, WZ63, and WZ91.

As shown in figure 8, the surface morphology of four extruded alloys soaked in 3.5%NaCl solution for 1 h is SEM. It can be seen that the corrosion products first appear at the junction of LPSO phase and Mg matrix. This is because of the potential difference between the second phase of magnesium alloy and the magnesium matrix, so the corrosion microelectricity formed with the magnesium matrix is occasionally corroded first. In addition, in the figure, the corrosion products in WZ63 and WZ91 alloys are more and the particles are larger, while the corrosion products in WZ93 and WZ61 alloys are less and the particles are smaller. In particular, there are almost no corrosion products on the surface of WZ93 alloy. It can be further shown that the corrosion resistance of WZ93 alloy is the best, which is consistent with the results of polarization curve and impedance spectrum.

Generally speaking, in addition to promoting the galvanic corrosion of magnesium alloys, the second phase in magnesium alloys can also act as a corrosion barrier to hinder the corrosion of alloys [24]. Whether accelerated corrosion or hindered corrosion depends on the quantity and distribution of the second phase. The



Y/Zn mass ratio determines the type of the second phase in the alloy. When the Y/Zn mass ratio is fixed, the total number of Y and Zn atoms determines the volume fraction of LSPO in the alloy, and the width of LSPO phase also changes with the total number of Y and Zn atoms. The volume fraction of LPSO phase in WZ93 alloy is the largest, and the long strip LPSO phase is relatively wide, and the distance between phases is narrow. When the alloy is immersed in NaCl solution, the continuous strip LPSO phase is distributed intensively. The alloy surface reduces the reaction area of the alloy surface. Because of its very low corrosion rate, it becomes an effective obstacle to alloy corrosion. Literature [25] think LPSO phase in the magnesium alloy surface is a layer of passivation film, the passive film in a relatively wide range of pH value is stable, can be as a semiconductor, which severely restrict ions in and out of the channel, but relatively easy to make an electron or a hole through, so that the existence of the passivation membrane can effectively block the solute transport process in the solution, such as metal ions ( $Mg^{2+}$ ) into the solution of the rate, when  $Mg^{2+}$  into the solution of the rate of less than the rate of migration of electrons from the anode to cathode, anode process is restrained, metal dissolution rate is reduced, in addition, The contact of the active anion (such as  $Cl^{-}$ ) in the corrosive medium with  $\alpha$ -Mg through hydroxides or oxide films is also hindered, all of which inhibit the electrode reaction and chemical reaction, thus improving the corrosion resistance of the alloy. When the volume fraction of LPSO phase in the alloy decreases, this blocking ability weakens, so the corrosion resistance of the four extruded alloys increases with the volume fraction of LPSO phase.

### 3. Conclusion

In this paper, by studying the microstructure, mechanical properties and corrosivity of four extruded Mg-Y-Zn alloys with specific Y/Zn (wt%) Ratios, the following main conclusions are drawn:

- 1) The Y/Zn mass ratio determines the type of the second phase in the alloy. When the Y/Zn mass ratio is fixed, the total number of Y and Zn atoms determines the volume fraction of LSPO in the alloy.
- 2) WZ63 alloy is composed of Mg matrix, W phase and lpsO phase. With the increase of Y/Zn mass ratio, the W phase disappears. The volume fraction of LPSO phase increased first and then decreased in the four alloys, and the volume fraction of LPSO phase was the largest in WZ93 alloy. 18R-LPSO structure and 14H-LPSO structure exist in extrusion alloy at the same time.
- 3) The ultimate tensile strength and elongation of WZ93 alloy are 327 MPa and 23%, respectively. Compared with other extruded alloys, it has good comprehensive mechanical properties. This is mainly due to the content of LSPO phase with the largest volume fraction in the alloy. Compared with magnesium alloy, LSPO plays a role of strengthening and refining grains, which can improve the strength of the alloy. At the same time, the large lpsO phase in WZ93 alloy reduces the interface between the two phases and the probability of crack initiation.

- 4) The corrosion resistance of the four extrusion alloys increased with the increase of the volume fraction of the LPSO phase in the alloy. On the one hand, the strip-like LSPO phase with continuous structure distributed on the alloy surface not only plays a cathode role in the micro current corrosion, but also acts as a barrier to corrosion. On the other hand, a passivation film is formed on the surface of LSPO phase in magnesium alloy, which can effectively block the transport process of solute in solution.

## Acknowledgments

The authors gratefully acknowledge the Scientific and Technological Innovation Programs of Higher Education Institutions in Shanxi (grant No. 2019L0655), the Natural Science Foundation of Shanxi Province (grant No. 201901D211310), Transformation of Scientific and Technological Achievements Programs of Higher Education Institutions in Shanxi (TSTAP), Science and Technology Major Projects of Shanxi Province (20191102004), Key Scientific Research Project in Shanxi Province (201903D111008), Central Special Funds Guiding the Development of local Science and Technology (grant No. YDZX20181400002967), and the Collaborative Innovation Center of Shanxi Key Basic Materials.

## ORCID iDs

Baosheng Liu  <https://orcid.org/0000-0002-3670-3467>

## References

- [1] Zhou M, Liu C, Gao Y, Xu S and Jiang S 2019 *The Chinese Journal of Nonferrous Metals* **1** 18–20
- [2] Ji Y, Li D, Zeng X and Ding W 2018 *Journal of Materials Science & Engineering* **36** 14–20
- [3] Shi Q-xin, Wang C-ju, Deng K-kun, Nie K-bo, Cao M, Gan W-min and Liang W 2020 *Mater. Sci. Eng. A* **772** 138827
- [4] Yang Z, Li J P, Zhang J X, Lorimer G W and Robson J 2008 *Acta Metallurgica Sinica* **21** 313–28
- [5] Wu G, Sun M, Wang W and Ding W 2010 *The Chinese Journal of Nonferrous Metals* **20** 1021–31
- [6] Gao H Y, Ikeda K, Morikawa T, Higashida K and Nakashima H 2013 *Materials Transactions* **54** 632–5
- [7] Wan D, Li J and Yu T 2015 *Rare Metal Materials and Engineering* **44** 2651–5
- [8] Tahreen N, Zhang D F, Pan F S, Jiang X Q, Li D Y and Chen D L 2015 *Journal of Materials Science & Technology* **31** 1161–70
- [9] Zhang Z, Li X, Wang Z, Le Q, Hu W, Bao L and Cui J 2015 *Materials and Design* **88** 915–23
- [10] Zhu Y M, MORTON A J and Nie J F 2010 *Acta Materialia* **58** 2936–47
- [11] Gröbner J, Kozlov A, Fang X Y, Geng J, Nie J F and Schmid-Fetzer R 2012 *Acta Materialia* **60** 5948–62
- [12] Wang J, Gao S, Song P, Huang X, Shi Z and Pan F 2011 *Journal of Alloys and Compounds* **509** 8567–72
- [13] Itoi T, Inazawa T, Yamasaki M, Kawamura Y and Hirohashi M 2013 *Materials Science & Engineering A* **560** 216–23
- [14] Zhang Z, Liu X, Hu W, Li J, Le Q, Bao L, Zhu Z and Cui J 2015 *Journal of Alloys and Compounds* **624** 116–25
- [15] Zhao X, Shi L and Xu J 2013 *Materials Science and Engineering C* **33** 3627–37
- [16] Li C Q, Xu D K, Zeng Z R, Wang B J, Sheng L Y, Cheng X B and Han E H 2017 *Materials & Design* **121** 430–41
- [17] Xu D, Han E and Xu Y 2016 *Progress in Natural Science: Materials International* **26** 118–20
- [18] Tong L B, Li X H and Zhang H J 2013 *Materials Science & Engineering A* **563** 177–83
- [19] Oñorbe E, Garcés G, Dobes F, Pérez P and Adeva P 2013 *Metallurgical and Materials transactions A* **44** 2869–83
- [20] Liu H, Huang H, Li C and Yang X 2017 *Material Science and Engineering* **40** 35–7
- [21] Cheng P, Zhao Y, Lu R and Hou H 2018 *Journal of Alloys and Compounds* **764** 226–38
- [22] Guo Y, Wang Y, Wang Q, Dong Z, Wang L, Fang D and Liu B 2018 *Rare Metal Materials and Engineering* **47** 2533–4
- [23] Song Y, Han E, Dong K, Shan D, Yim C D and You B S 2014 *Corrosion science* **88** 215–25
- [24] Pérez P, Cabeza S, Garcés G and Adeva P 2016 *Corrosion Science* **107** 107–12
- [25] Liu Z, Zhu X, Zhou G and Li J 2012 *Journal of Chinese Society for Corrosion and Protection* **32** 479–84
- [26] Yang K, Zhang J, Zong X, Wang W, Xu C, Cheng W and Nie K 2016 *Materials Science & Engineering A* **669** 340–3